Supplementary materials:

Hollow sphere structured Co$_3$V$_2$O$_8$ as a half-conversion anode material with ultra-high pseudocapacitance effect for potassium ion batteries

Fei Chen, Shuo Wang, Yi-Xuan Li, Kuo Cao, Chun-Hua Chen *

CAS Key Laboratory of Materials for Energy Conversions, Department of Materials Science and Engineering& Collaborative Innovation Center of Suzhou Nano Science and Technology, University of Science and Technology of China, Anhui Hefei 230026, China
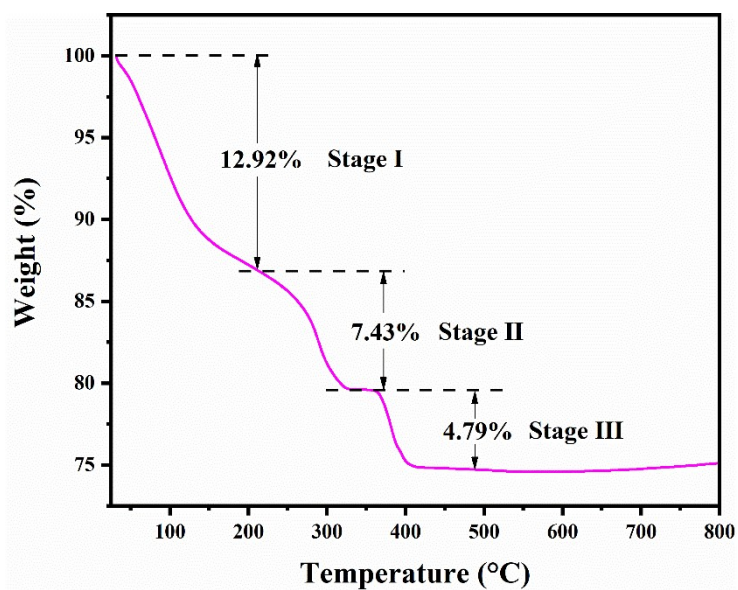
*Address correspondence to cchchen@ustc.edu.cn

Fig S1. TG curve of Co-V-precursor measured in air. Stage I: loss of adsorbed water; Stage II: carbonization of organic components; Stage III: combustion of carbon.
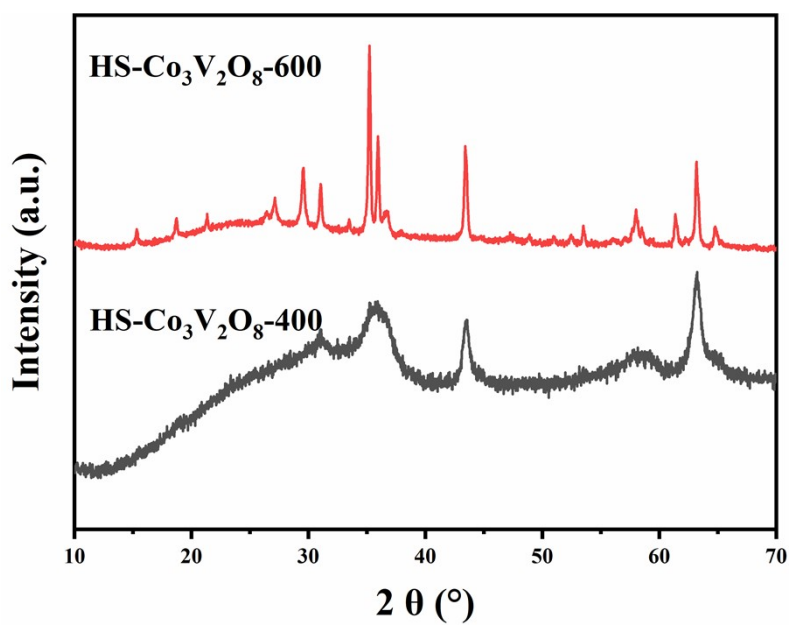

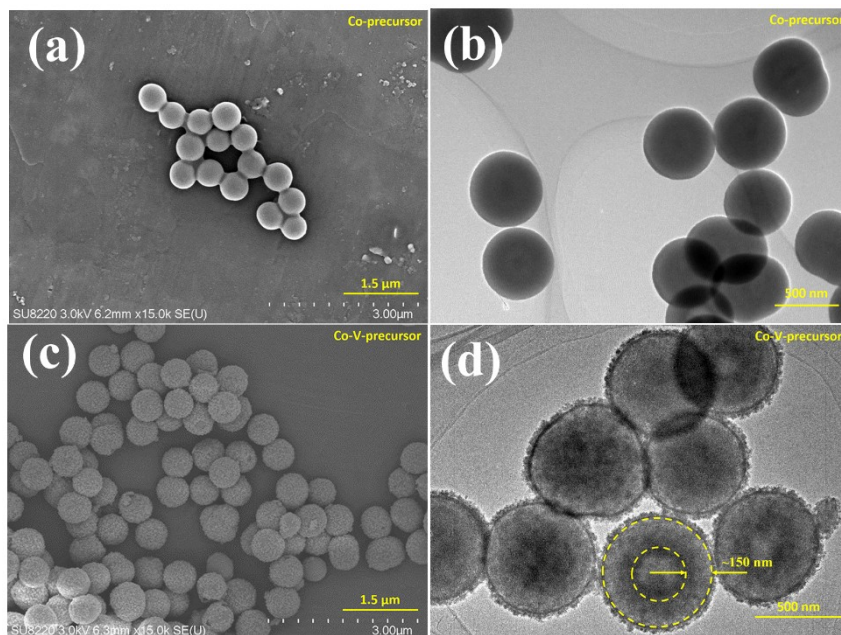**Fig S2.** XRD patterns of HS-$Co_3V_2O_8$ calcined at 400°C and 600°C.

Fig S3. SEM and TEM images of Co-precursor (a-b) and Co-V-precursor (c-d).
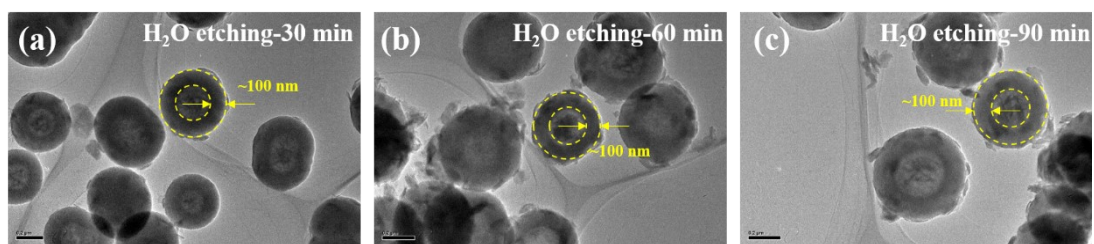

Fig S4. TEM images of Co-precursor reflux for different time under water etching without the addition of NH_4VO_3.
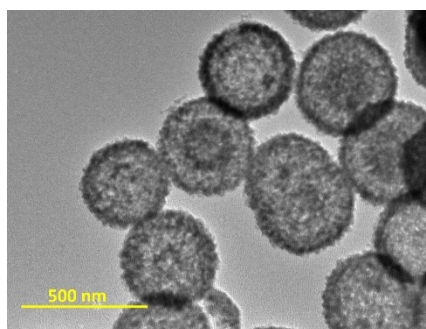

Fig S5. TEM image of HS-$Co_3V_2O_8$-400.

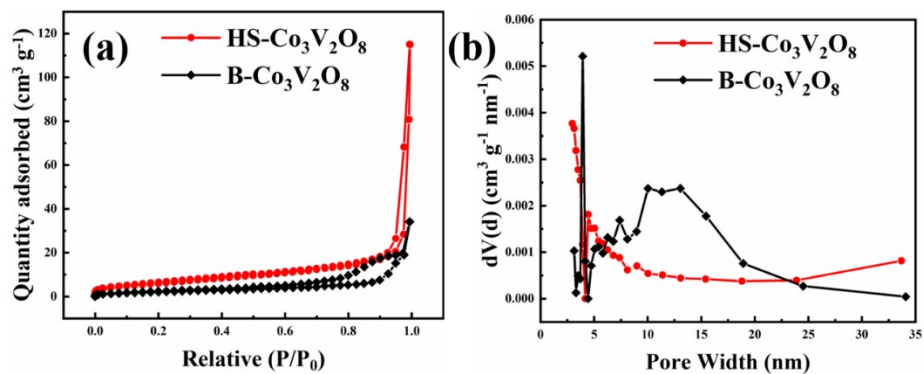**Fig S6.** Nitrogen adsorption-desorption isotherms (a) and the pore size distributions (b) of HS-$Co_3V_2O_8$ and B-$Co_3V_2O_8$.
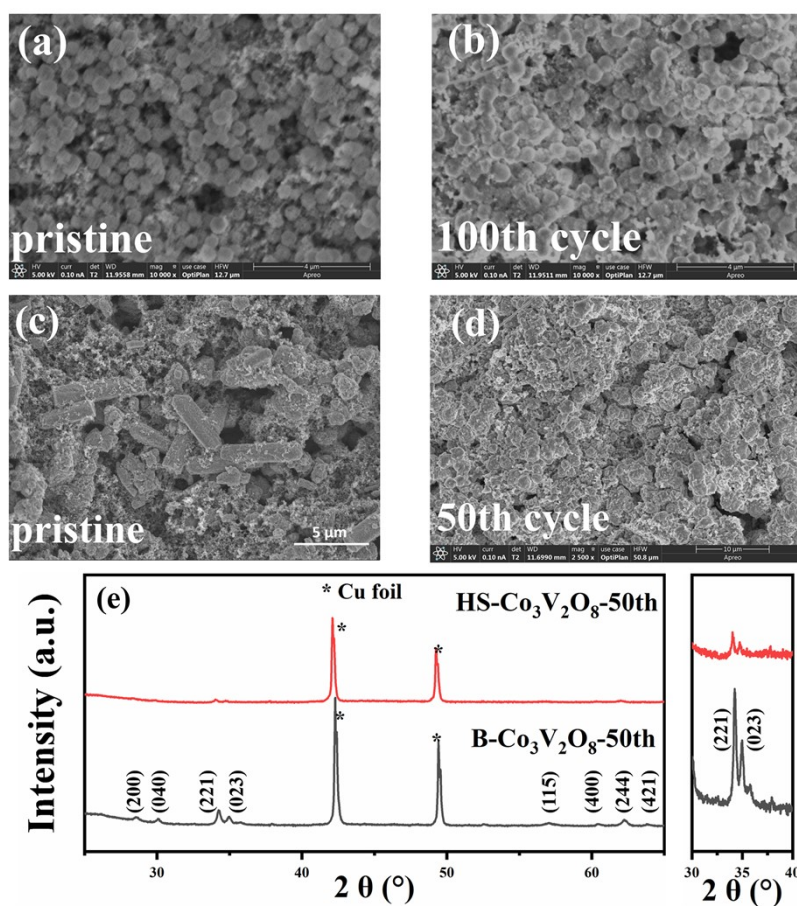
Fig S7. SEM images of HS-$Co_3V_2O_8$ electrode before (a) and after (b) 100 cycles (current density: 100 mA g^{-1}); B-$Co_3V_2O_8$ before (c) and after (d) 50 cycles (current density: 100 mA g^{-1}); XRD patterns of HS-$Co_3V_2O_8$ and B-$Co_3V_2O_8$ electrode after 50 cycles (e).
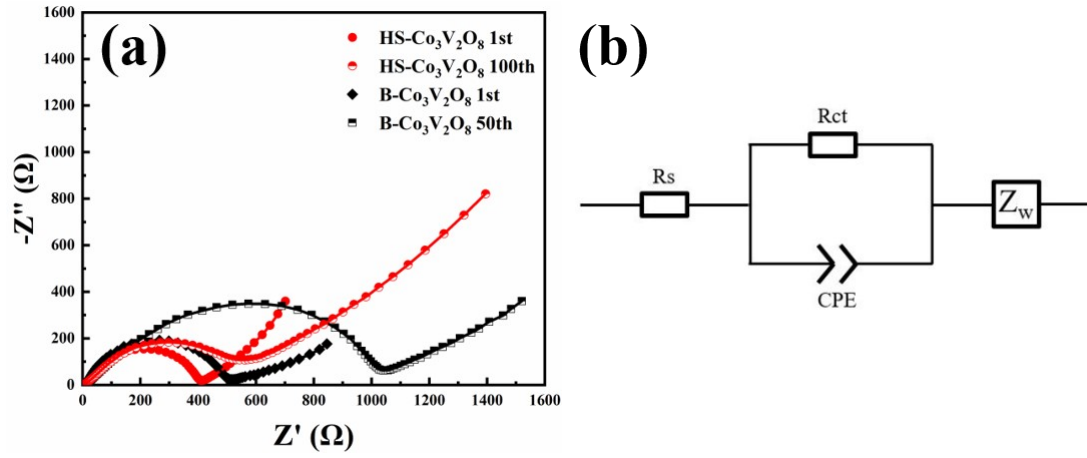
Fig S8. (a) EIS spectra of HS-Co$_3$V$_2$O$_8$ and B-Co$_3$V$_2$O$_8$ samples; (b) the equivalent circuit used for the experimental impedance data.

Table S1. The fitted impedances of HS-Co$_3$V$_2$O$_8$ and B-Co$_3$V$_2$O$_8$.

sample		Rs (Ω)	Rct (Ω)
B-Co$_3$V$_2$O$_8$	pristine	6.314	417.4
	50th cycle	8.092	953.3
HS-Co$_3$V$_2$O$_8$	pristine	8.264	347.4
	100th cycle	7.238	626.9

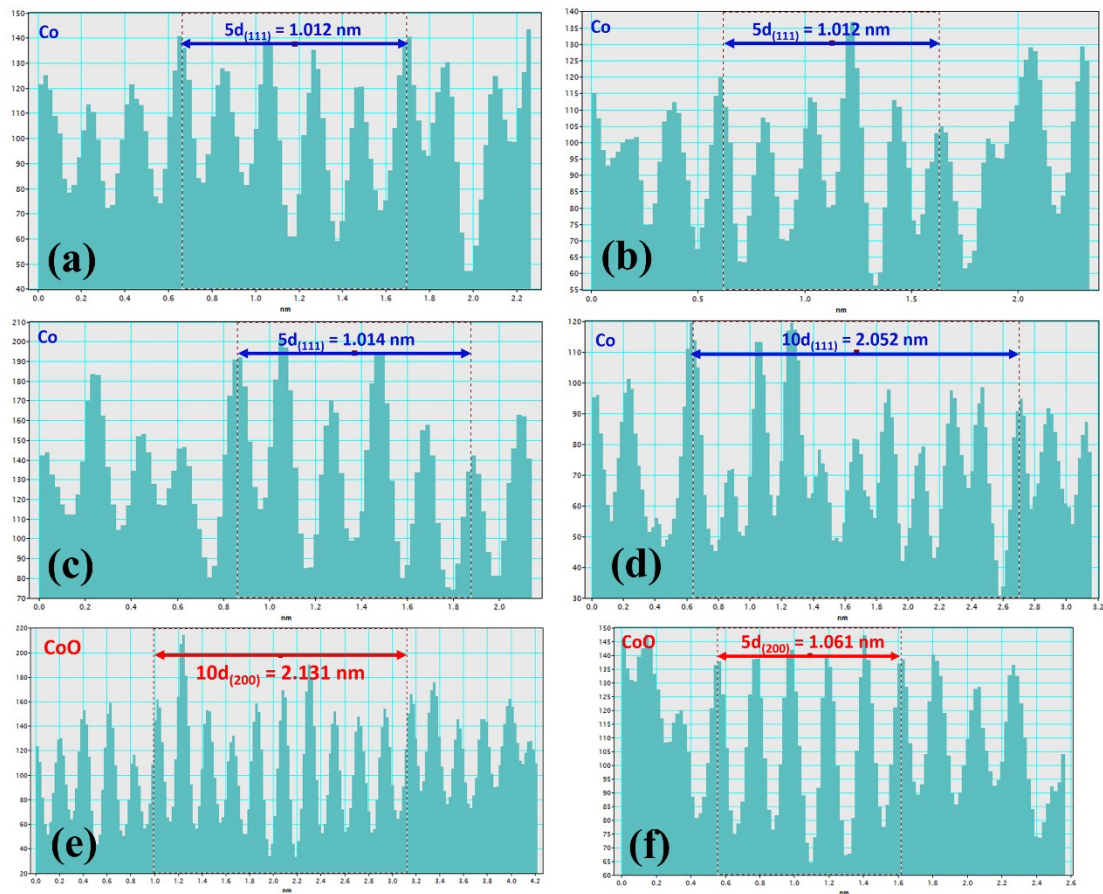**Fig S9.** relevant intensity profiles for the line scans across the lattice fringes of Fig. 5b: "Co-2" region in Fig. 5b (a); "Co-3" region in Fig. 5b (b); "Co-4" region in Fig. 5b (c); "Co-5" region in Fig. 5b (d); "CoO-1" region in Fig. 5b (e); "CoO-2" region in Fig. 5b (f).

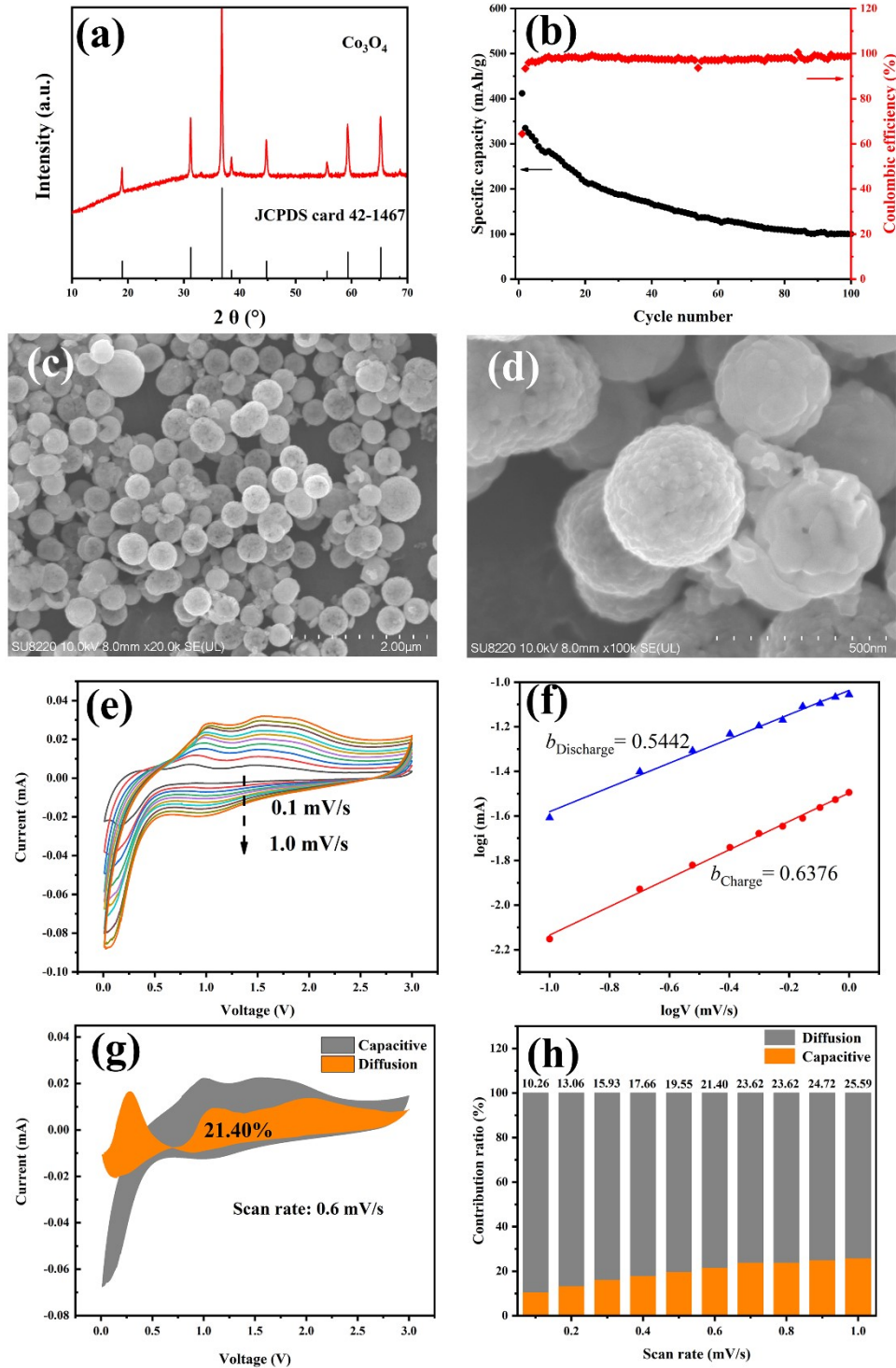**Fig S10.** Analyses of Co_3O_4 electrode: XRD patterns of Co_3O_4 (a); Cycle performance at 100 mAh g^{-1} (b); SEM images of Co_3O_4 (c and d); CV curves of Co_3O_4 electrode at different scan rates (e); The *b* values of charge and discharge peak of Co_3O_4 (f); The contribution percentages from capacitive and diffusion effect of Co_3O_4 electrode at 0.6 mV s^{-1} (g) and other scan rates (h).

In order to verify the advantages of binary metal oxides, we obtained Co_3O_4 by sintering Co-precursor directly in air for 2h. Fig. S10a indicates that the powder belongs to the Fd-3m space group and has good crystallinity. Fig. S10c and S10d exhibit SEM images under different magnifications. It can be seen that (Fig. S10c) some spheres have been broken under high temperature treatment. And the enlarged image (Fig. S10d) shows that the pore distribution on the nano-spheres surface is less than HS-$Co_3V_2O_8$, which may affect the specific surface area of the material. Afterwards, we performed electrochemical analysis on Co_3O_4. The initial charge capacity at 100 mA g^{-1} can reach 411 mA h g^{-1}, but only 99.9 mA h g^{-1} remains after 100 cycles, with a capacity retention rate of 24.3% (Fig. S10b). The poor cycle stability can be attributed to the fragmentation of particles caused by the huge volume change during cycling. Meanwhile, the contribution of pseudocapacitive adsorption to the charging and discharging process is calculated through the CV curves at different scan rates. The contribution ranges from 10.26% at 0.1 to 25.59% at 1.0 mV s^{-1}, which is at a relatively low level. The difference between Co_3O_4 and HS-$Co_3V_2O_8$ in pseudocapacitive adsorption may be due to the difference in porosity.
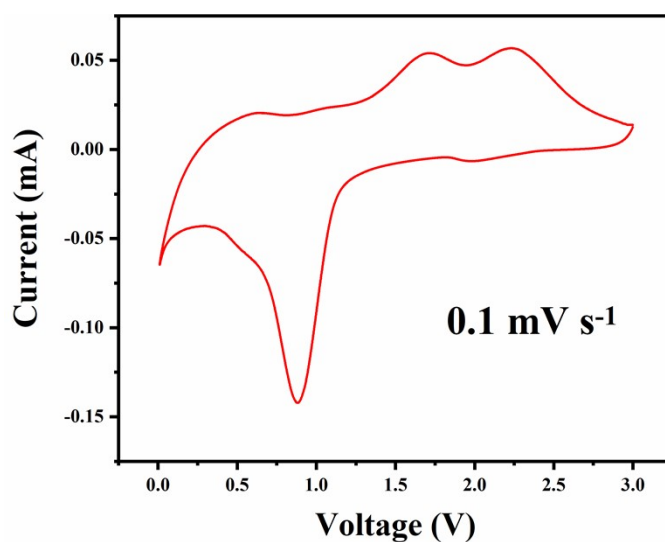

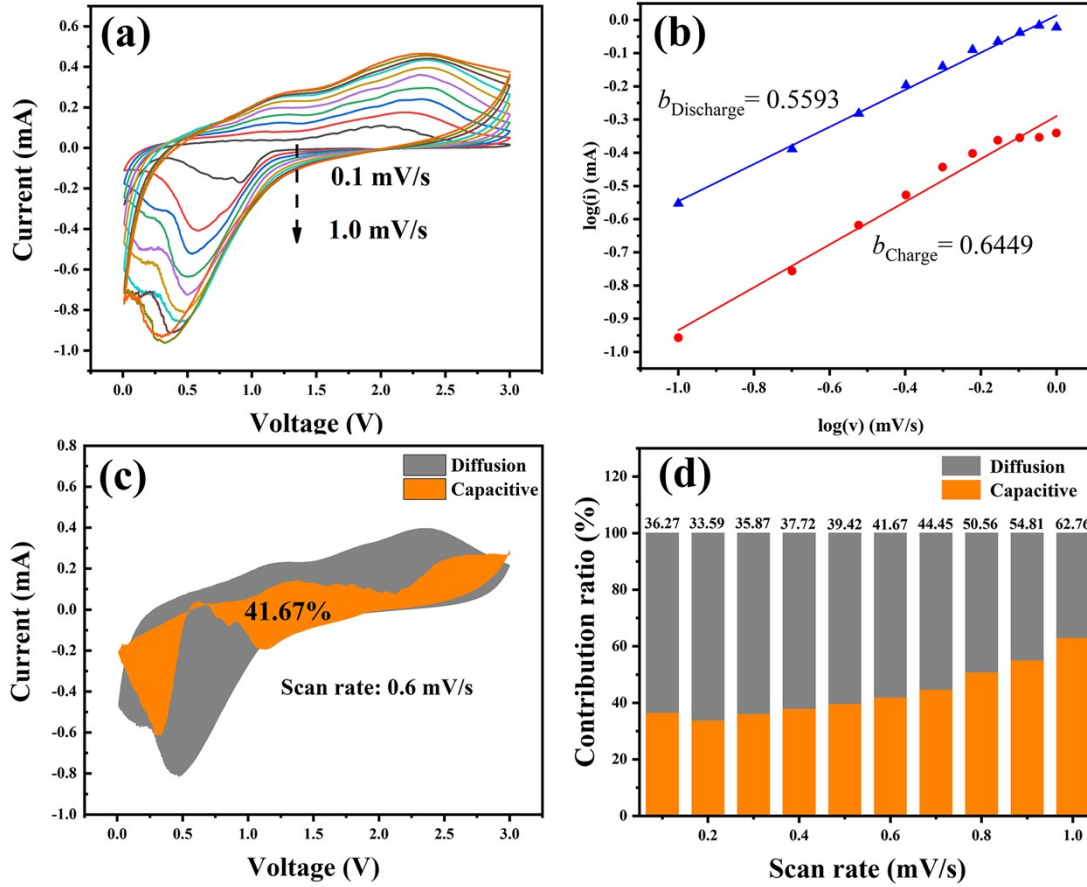**Fig S11.** The CV curve of HS-$Co_2V_3O_8$ electrode at 0.1 mV s^{-1}.

Fig S12. Electrochemical analyses of B-$Co_3V_2O_8$ electrode: CV curves of B-$Co_3V_2O_8$ electrode at different scan rates (a); The *b* values of charge and discharge peak of B-$Co_3V_2O_8$ (b); The contribution percentages from capacitive and diffusion effect of B-$Co_3V_2O_8$ electrode at 0.6 mV s^{-1} (c) and other scan rates (d).

Table S2. Comparison of recent reported conversion anode materials for PIBs.

Materials	Current: mA g^{-1}	Capacity: mA h g^{-1}	Cycle number/Capacity Retention	Ref.
HS-$Co_3V_2O_8$	20, 50, 100, 200, 400	409, 379, 333, 291, 267	100 / 82.0%	This work
SNF-VS_2	25, 50, 100, 200, 500	382, 281, 244, 167, 105	500 / 93.3%	28

$Zn_3V_3O_8$	50, 100, 200, 500, 1000	286, 136.9, 87.1, 57.6, 43.6	100 / 41.8%	20
$(NH_4)_2Mo_3S_{13}$	100, 200, 500,1000	302, 230, 150, 80	100 / 33.9%	29
Yolk–shell structured $CoSe_2/C$	50, 100, 200, 300, 500, 800, 1000	362.4, 261.1, 247.3, 239, 206.7, 197, 186.4	200 / 63.6%	30
$MoSe_2/N-C$	100, 200, 500, 1000, 2000	300, 244, 211, 195, 178	300 / 92.7%	31
$FeVO_4$	100, 200, 300, 500, 1000, 2000	300, 280, 260, 240, 220, 190	2000 / 97.2%	24

$Zn_3V_3O_8$

$(NH_4)_2Mo_3S_{13}$